AIAA JOURNAL
Vol. 43, No. 3, March 2005

Correlation-Based Image Registration for Applications Using Pressure-Sensitive Paint

Sang-Hyun Park* and Hyung Jin Sung†
Korea Advanced Institute of Science and Technology, Daejeon 305-701, Republic of Korea

A new algorithm, named correlation-based image registration, was developed to improve the resolution of image registration for applications using pressure-sensitive paint. The local displacement vectors were obtained by finding the displacement that maximized the cross correlation between two interrogation windows obtained under wind-off and wind-on conditions. A layer of speckle was sprayed to apply the cross-correlation method in a small interrogation window, without requiring identification of control points as used in the conventional method. Recursive multigrid processing was employed to increase the nonlinear spatial resolution. Several interpolation methods for the image transformation procedure were evaluated: windowed-sinc interpolation was the most accurate, and 4 × 4 cubic interpolation was the most efficient.

Nomenclature

A, B, C	=	Stern–Volmer constant
h	=	interpolation kernel
I	=	luminescent intensity
N	=	interpolation kernel size
P	=	pressure
R	=	cross-correlation function
w	=	window function in sinc kernel
δ	=	displacement
ε	=	relative error

Subscripts

ref	=	reference condition
reg	=	registered condition

I. Introduction

A CAPABILITY to measure air pressure using pressure-sensitive paint (PSP) has improved significantly in recent decades. PSP is a luminescent surface coating whose luminescence intensity is related to the surface air pressure. The main advantage of the PSP technique is that it can provide continuous field measurement with a high spatial resolution as opposed to the discrete point measurement possible with conventional pressure taps or transducers. Because the use of PSP can eliminate the need for many pressure taps, wind-tunnel models can be constructed more rapidly and at lower cost.[1]

The most common technique of measuring the surface-pressure distribution using PSP utilizes the ratio of image intensities obtained under wind-off and wind-on conditions. This technique greatly reduces the undesirable effects of nonuniform coating thickness and nonuniform illumination. However, significant errors in the intensity ratio can be induced if there is a small displacement or deformation of the surface between the two images.[2] Accurate acquisition of the pressure distribution using the intensity ratio requires that such displacement and deformation of the model be corrected. This process of rearranging the pixels is called image registration.[3]

Presented as Paper 2004-882 at the AIAA 42nd Aerospace Sciences Meeting, Reno, NV, 5–8 January 2004; received 16 January 2004; revision received 8 July 2004; accepted for publication 18 August 2004.

*Ph.D. Candidate, Department of Mechanical Engineering, 373-1 Guseong-dong, Yuseong-gu. Member AIAA.

†Professor, Department of Mechanical Engineering, 373-1 Guseong-dong, Yuseong-gu; hjsung@kaist.ac.kr. Member AIAA.

A single global transform between the wind-off and wind-on images is generally used for rearranging the pixels. A transform function is obtained by measuring the displacement of prior known points on the model surface, that is, control points. The use of a single transform function in this conventional image-registration technique is less accurate when the model motion contains nonlinear local deformation or warping. Moreover, the identification of the control points is a significant bottleneck in the image-registration process. Because an error in the location of a single control point can significantly influence the transformed image, it is important to precisely identify and link the control points between the wind-off and wind-on images.

The present study involved the development of a new algorithm to improve the resolution of the image registration; this algorithm is named correlation-based image registration (CBIR). The core of CBIR is as follows. An image plane is divided into $n \times n$ pixels, that is, interrogation windows. In each interrogation window, the displacement vectors for the local motion of the model are obtained by calculating the maximum cross correlation between the wind-off and wind-on images. Note that the CBIR method can describe the local motions of the model without the use of control points. Instead, a layer of speckle is sprayed to apply the cross-correlation method in a small interrogation window. Recursive multigrid processing is employed to increase the nonlinear spatial resolution. To optimize the subpixel accuracy in the image transformation procedure, several interpolation methods are evaluated: nearest neighbor, bilinear, B-spline, cubic, and sinc.

II. Image Registration

A. Stern–Volmer Relation

The quenching of luminescence by oxygen means that the luminescent intensity I emitted from PSP is inversely proportional to air pressure P, according to the Stern–Volmer relation

$$I_z/I = 1 + K_p P \tag{1}$$

where I_z is the luminescent intensity in the absence of oxygen (vacuum condition) and K_p is the Stern–Volmer constant. Hence, the air pressure P can be determined by detecting the luminescent intensity I of the PSP. However, the luminescent intensity in the absence of oxygen I_z cannot be easily obtained in wind-tunnel testing, and hence another version of the Stern–Volmer relation is introduced, which uses the ratios of intensity and pressure:

$$I_0/I = A + B(P/P_0) \tag{2}$$

where I_0 and P_0 are the reference luminescent intensity and pressure at a known temperature of the wind-off condition, and A and B are the calibration coefficients. In this paper, a modified second-order

Stern–Volmer relation is employed to obtain more accurate PSP data reduction[4];

$$I_0/I = A + B(P/P_0) + C(P/P_0)^2 \tag{3}$$

where C is another calibration coefficient.

B. Conventional Methods

Image registration is required to correct possible misalignment between the wind-off and wind-on images. When the wind-off image $I_0(x, y)$ and the wind-on image $I(x', y')$ are given, where (x, y) and (x', y') are the image-plane coordinates, it is necessary to find the relation between (x, y) and (x', y') that aligns the image of the object in I with that in I_0. Such a relation is called the transform function.

A general approach is to use a transform that takes the form of a general polynomial series expansion:

$$x = \sum_{i,j=0}^{n} a_{i,j} x'^i y'^j \qquad (i + j \le n) \tag{4}$$

$$y = \sum_{i,j=0}^{n} b_{i,j} x'^i y'^j \qquad (i + j \le n) \tag{5}$$

The usual way to determine the coefficients is to measure the image coordinates (x, y) and (x', y') of the control points. In Eqs. (4) and (5), the number of unknown coefficients is $2({}_{n+2}C_2)$, and the required minimum number of control points for solving these equations is ${}_{n+2}C_2$ in the form of combination formula. The solutions of these equations are valid not only for rigid-body motion but also for elastic deformation of the model. Once the coefficients are obtained, the intensity of each pixel in the original image is displaced to the transformed image by the transform function. If the model movement includes nonlinear local deformation or warping, it is difficult to describe the model motion with lower-order polynomials. Although the use of higher-order polynomials appears to make the transform more accurate, the improvement of accuracy is confined as a result of their unstable nature.

Overcoming the just-stated limitations requires the use of image registration using local information. For example, Shanmungasundaram and Samareh-Abolhassani[5] developed a method employing Delaunay triangulation. In this method, the image is divided into triangular patches, and then the pixels inside the patches are transformed parametrically. This approach can give an accurate result even when local deformations are present, but it requires the exact matching of many control points between the wind-off and wind-on images via Delaunay triangulation.

It is important to identify the control points exactly and to link the corresponding control points between the wind-off and wind-on images precisely because locating a single control point can have a global effect on the transformed image. Several automatic algorithms have been developed,[6] but few are robust enough to be useful.[1] Identification of control points represents the principal bottleneck for automated PSP data reduction. To remove the need for such points, Weaver et al.[7] proposed a quantum pixel-energy distribution algorithm with spatial anomalies used for embedded control points. They applied an aerosol mist of gray paint over the base coat before the application of the PSP top layer. In this method, the image is shifted pixel by pixel until the total count difference between all pixels in the two images is minimized. However, this process is very time consuming, and optimizing the algorithm is difficult.

C. Correlation-Based Image Registration

Maximizing the cross correlation between two images is widely used to estimate the motion of an object. This is the main principle of particle image velocimetry to measure the velocity of flowfield.[8–10] However, here the correlation method is not applied directly because of the inherent intensity variations between "wind-off" and "wind-on" images. To eliminate their effect, a detective distinction is needed to maximize the image correlation. In the present study, a layer of speckle is coated by spraying gray paint coarsely over the base coat with a high-pass filtering process.

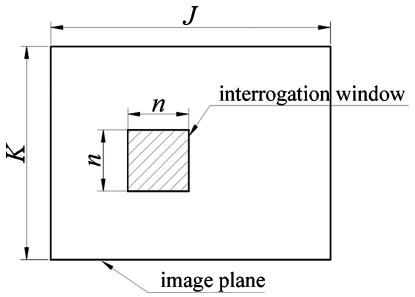

Fig. 1 Image plane and interrogation window.

The present CBIR method divides an image plane into squares of $n \times n$ pixels representing interrogation windows (Fig. 1). In each interrogation window, the displacement vector is obtained to represent the local motion of the object by calculating the cross correlation in Eq. (6):

$$R(u, v) = \frac{\sum_{j=1}^{J}\sum_{k=1}^{K} I_1(j,k)\cdot I_2(j-u, k-v)}{\sqrt{\sum_{j=1}^{J}\sum_{k=1}^{K} I_1^2(j,k)}\cdot\sqrt{\sum_{j=1}^{J}\sum_{k=1}^{K} I_2^2(j-u, k-v)}} \tag{6}$$

The displacement of an interrogation window in the wind-on image is equivalent to the displacement of the peak in the cross-correlation plane between the wind-off and wind-on images.

To save time when computing the cross correlation, a fast Fourier transform (FFT) is applied to windows in the wind-off and wind-on images with the same size and position, and hence dimension n is made an mth power of 2. The displacement of pixels inside the interrogation window is linearly interpolated with the displacement vectors of the four nearest windows. This process can be summarized as follows:

1) A high-pass filtering process is applied to the original wind-off and wind-on images.

2) The wind-off and wind-on images are divided into two interrogation windows of size $n \times n$, where n is an mth power of 2.

3) The FFT of both windows is calculated.

4) The cross product of the wind-off image and the conjugate wind-on image is computed in the Fourier domain.

5) The inverse FFT of the cross product is calculated.

6) The location of maximum correlation is determined, and the displacement of this location from the center becomes the displacement vector of the window.

7) The displacement vectors of pixels inside the interrogation window are calculated by interpolating linearly with the displacement vectors of the four nearest interrogation windows.

8) The wind-on image is transformed pixel by pixel along the determined displacement vectors.

If the model motion is highly nonlinear, it is desirable to reduce the window size to minimize the linear interpolation error and to describe the local deformation precisely. However, the loss of speckle pairs caused by the same window size and position of two interrogation windows makes the simple correlation unsuitable for a small window. To prevent aliasing of the FFT, the minimum window size must be larger than four times the window displacement. To overcome this problem, recursive multigrid processing with discrete window offset[11] is applied in this study. The main idea of this method is to shift the window of the wind-on image on the basis of predicted displacement. When the displacement vector $\delta = (\delta x, \delta y)$ is estimated, the window of the wind-on image can be selected with a relative offset in order to maximize the cross correlation. The result obtained with coarse windowing is used as a predictor of the displacement vector (Fig. 2). Finer windowing is then performed by halving the windows in both directions, and the predictor is applied to the window offset by means of simple substitution of the result of the previous iteration. This process makes it possible to achieve

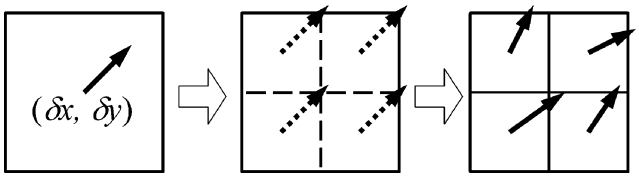

Fig. 2 Application of a coarse result to build a finer predictor.

both high spatial resolution and high accuracy. The process involves the following steps:

1) The aforementioned standard correlation method is applied using relatively coarse interrogation windows.

2) The resultant displacement vectors of the coarse windows are used as a predictor of finer windows.

3) The window size is reduced by halving the windows in both directions.

4) The finer windows of the wind-on image are shifted along the predictor.

5) The displacement vectors of the finer windows are corrected by calculating the correlation.

6) The calculated displacement vectors of the finer windows are validated with respect to appropriate error criteria.

7) The validated displacement distribution is then used as a final output or as a recursive input to step 2. The interrogation process is repeated until a convergence criterion is satisfied.

The data validation scheme applied in step 6 was median filtering, which is frequently used in image processing to remove binary noise. In this scheme, a displacement value is compared with the median value in the neighboring pixels. If the difference exceeds predetermined threshold value, then the displacement vector is considered as an error vector.

D. Interpolation Methods

Applying the transform maps the intensity value at an original wind-on image plane $I(x', y')$ onto a transformed image plane at $I(x, y)$. In this procedure, an original image pixel does not align neatly on the transformed image coordinate, and hence it is necessary to use an interpolation technique to compute the exact intensity value to be placed at location (x, y) on the transformed image plane. This reconstruction of a continuous signal from discrete points can be considered as a convolution operation[12]:

$$I(x, y) = \sum_{i,j} I(i, j)h(x - i, y - j) \tag{7}$$

Usually, symmetrical and separable interpolation kernels are used to reduce the computational complexity:

$$h(x, y) = h(x)h(y) \tag{8}$$

In the present study, six interpolation methods were evaluated: 1) nearest neighbor, 2) linear, 3) B-spline, 4) cubic, 5) truncated sinc, and 6) windowed sinc. The simplest is nearest-neighbor interpolation, in which the intensity value closest to (x, y) is assigned to the transformed pixel. Whereas this is a computationally efficient procedure, a spatial offset error of as much as $1/\sqrt{2}$ pixel units is invoked:

$$h(x) = \begin{cases} 1, & 0 \le |x| \le 0.5 \\ 0, & \text{elsewhere} \end{cases} \tag{9}$$

Linear or separated bilinear interpolation involves interpolating linearly along each row of an image and then interpolating that result linearly in the columnar direction using four neighboring pixels. Although this approach can reduce the spatial offset error caused by the nearest-neighbor approach, the image is blurred by averaging the neighboring pixels, and more computation time is required:

$$h(x) = \begin{cases} 1 - |x|, & 0 \le |x| \le 1 \\ 0, & \text{elsewhere} \end{cases} \tag{10}$$

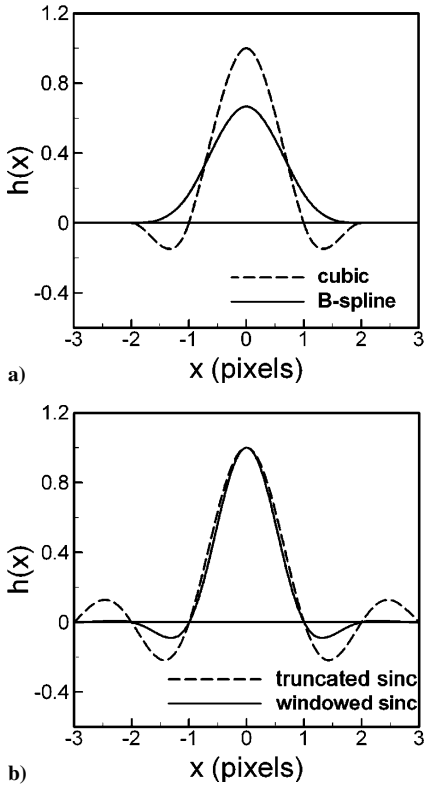

Fig. 3 Comparison of interpolation kernels: a) B-spline and cubic interpolations and b) truncated-sinc and windowed-sinc interpolations.

Higher-order interpolation methods are used to improve the quality of resampling. The most famous family of spline functions is B-splines, which are derived by several self-convolutions of a basis function. The cubic B-spline kernel is generally used in image processing (with the kernel size $N = 4$) and is shown in Fig. 3a (Ref. 13):

$$h(x) = \begin{cases} \frac{1}{2}|x|^3 - |x|^2 + \frac{2}{3}, & 0 \le |x| \le 1 \\ -\frac{1}{6}|x|^3 + |x|^2 - 2|x| + \frac{4}{3}, & 1 \le |x| \le 2 \\ 0, & \text{elsewhere} \end{cases} \tag{11}$$

Another popular higher-order interpolation method is cubic interpolation, which is also known as cubic convolution interpolation. This method uses cubic polynomials to construct an interpolation kernel. Here, cubic interpolation with different kernel sizes ($N = 4$ and 6) are compared:

$$h(x) = \begin{cases} (a+2)|x|^3 - (a+3)|x|^2 + 1, & 0 \le |x| \le 1 \\ a|x|^3 - 5a|x|^2 + 8a|x| - 4a, & 1 \le |x| \le 2, \quad a = -0.5 \\ 0, & \text{elsewhere} \end{cases} \tag{12}$$

$$h(x) = \begin{cases} \frac{6}{5}|x|^3 - \frac{11}{5}|x|^2 + 1, & 0 \le |x| \le 1 \\ -\frac{3}{5}|x|^3 + \frac{16}{5}|x|^2 - \frac{27}{5}|x| + \frac{14}{5}, & 1 \le |x| \le 2 \\ \frac{1}{5}|x|^3 - \frac{8}{5}|x|^2 + \frac{21}{5}|x| - \frac{18}{5}, & 2 \le |x| \le 3 \\ 0, & \text{elsewhere} \end{cases} \tag{13}$$

An ideal interpolation method involves multiplication with a rect function in the Fourier domain. This can be realized in the spatial domain by a convolution with the sinc function. From image sampling theory, this interpolation method allows reconstruction of the image without loss of information. However, this equation cannot be

applied to real images because the sinc function is nonzero to both positive and negative infinity. There are two common approaches used to overcome this drawback: truncation and windowing with a window function:

$$h(x) = \begin{cases} \dfrac{\sin(\pi x)}{\pi x} \cdot w(x), & 0 \le |x| \le \dfrac{N}{2} \\ 0, & \text{elsewhere} \end{cases} \tag{14}$$

The truncated-sinc kernel, $w(x) = 1$, exhibits excessive ripple in the passband resulting from the abrupt discontinuity at the ends of the truncated-sinc function. A simple method to improve the response is to use the sinc function with a shaping window to reduce the abruptness of the truncated ends. When using the three-term Blackman–Harris window, a smooth frequency response is returned:

$$w(x) = w_0 + w_1 \cos(2\pi x/N) + w_2 \cos(4\pi x/N) \tag{15}$$

where $N = 6$, $w_0 = 0.42323$, $w_1 = 0.49755$, and $w_2 = 0.07922$. The kernel shape of truncated- and windowed-sinc function is shown in Fig. 3.

III. Results and Discussion

A. Validation of the Concept

An air jet impinging on a flexible plate was used to illustrate the operation of the CBIR method. The plate material was vinyl film (thickness 0.13 mm), and its four corners were fixed loosely to ensure that some displacement and deformation occurred. The impinging angle was 45 deg, and the height was 1.5 times the nozzle diameter (6 mm). The exit velocity at the nozzle was 200 m/s. The PSP material used in this experiment was Uni-FIB (ISSI, United States), and a base coating of white enamel paint was sprayed beneath the PSP layer. As mentioned earlier, a layer of speckle was coated by an aerosol mist of gray paint. The illumination sources were two self-made light-emitting diodes with a center wavelength of 465 nm. The imaging device was a 16-bit cooled charge-coupled-device camera (Andor MCD434-BV, United Kingdom) with 1024×1024 pixels. A bandpass filter centered at 650 nm was positioned in the front of the camera lens. Raw images obtained in the wind-off and wind-on conditions with the impinging jet are shown in Fig. 4. Close inspection of Fig. 4 reveals that the speckles coated on the plate. A high-pass filtered wind-on image is shown in Fig. 4c. It is seen that the intensity variations were reduced, and high-frequency speckles were emphasized by the high-pass filtering process. A recommended number of speckle density, which ensures that the valid detection probability exceeds 95%, is larger than 6 (Ref. 14).

Arbitrary displacements and deformations were produced in the surface by the impinging jet, and the displacement vectors were obtained by the two methods indicated in Fig. 5: Fig. 5a, the standard correlation method; and Fig. 5b, the recursive multigrid method. The minimum size of the interrogation window was 32×32 pixels in the standard correlation method, whereas its size in the recursive multigrid method was reduced from 64×64 pixels to 8×8 pixels during three recursive loops. Accordingly, the spatial resolution of the recursive multigrid method was 16 times better than that of the standard correlation method.

Figure 6 shows a comparison of the intensity ratio between wind-off and wind-on conditions. With no image registration, it is almost impossible in Fig. 6a to recognize the pressure distribution of the impinging jet flow. However, in Figs. 6b and 6c clear images of the pressure distribution are obtained by image registration. In Fig. 6b, the image was registered by the second-order polynomial transform function with the automatic detection of 24 control points. In Fig. 6c, the image is shown to be well registered by the present CBIR method without using control points on the plate.

B. Performance Assessment

To evaluate the image-registration methods, the following relative error of the pixel mismatches between two images was obtained:

$$\varepsilon(j,k) = \left| \frac{I_{\text{reg}}(j,k) - I_{\text{ref}}(j,k)}{I_{\text{ref}}(j,k)} \right| \tag{16}$$

where I_{ref} is the reference intensity value and I_{reg} is the intensity value of the registered image. The mean relative error (MRE) is defined, which provides a measure for comparing the performance

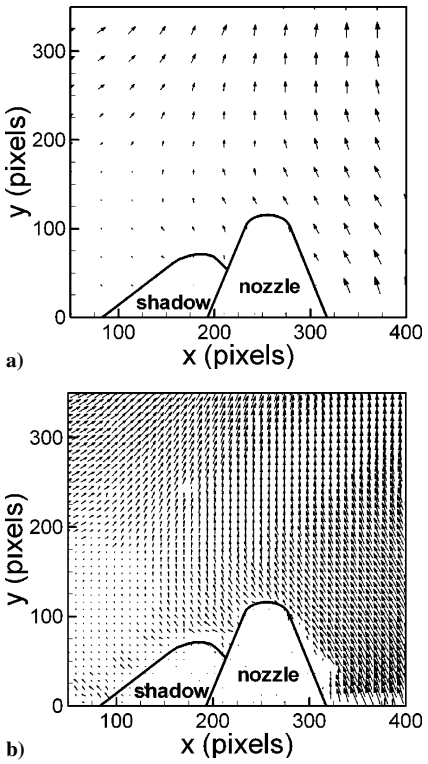

Fig. 5 Displacement vectors of interrogation windows: a) standard cross-correlation method and b) recursive multigrid method.

Fig. 4 Raw images of PSP with a speckle coat: a) wind-off, b) wind-on, and c) high-pass filtered images.

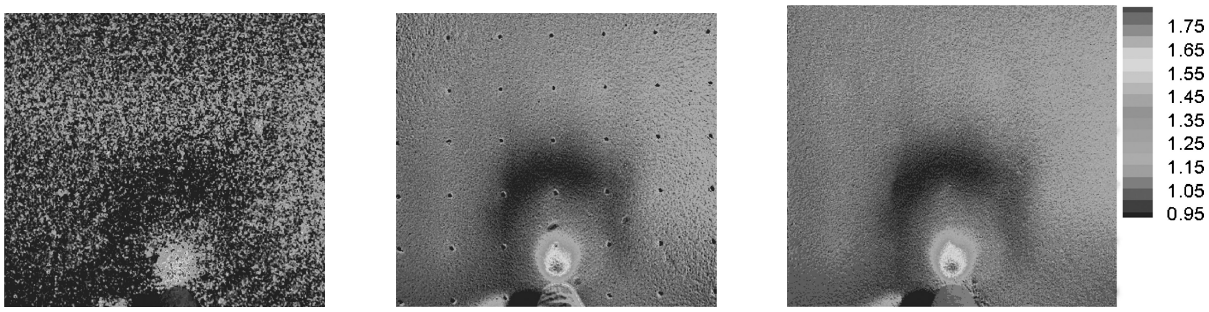

a) b) c)

Fig. 6 Intensity ratio of the impinging jet: a) no image registration, b) conventional method, and c) CBIR.

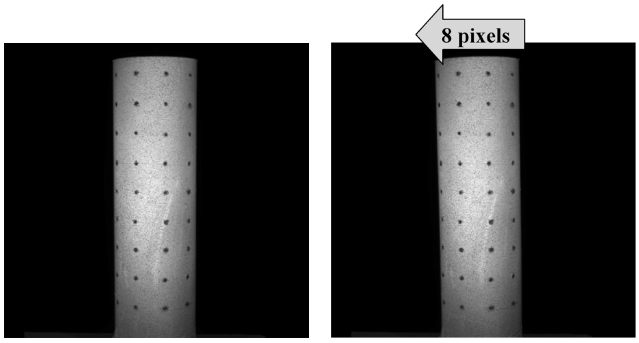

a) b)

Fig. 7 PSP-coated flexible cylinder with a speckle coat and control points: a) reference image and b) deformed image.

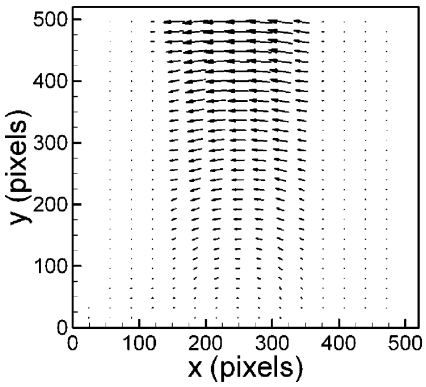

Fig. 8 Displacement vectors obtained by CBIR.

as a whole:

$$\mathrm{MRE} = \frac{1}{JK}\sum_{j=1}^{J}\sum_{k=1}^{K}\left|\frac{I_{\mathrm{reg}}(j,k) - I_{\mathrm{ref}}(j,k)}{I_{\mathrm{ref}}(j,k)}\right| \qquad (17)$$

Because the intensity under the wind-off condition is not the same as under the wind-on condition, the relative error between two images in Eq. (16) is not equivalent to the relative error of misregistration. Thus, in this study, artificial movement without the jet flow was imposed to compare the pixel-to-pixel intensity errors. Figure 7 shows two raw images for a PSP-coated flexible cylinder made of silicone. The bottom of the cylinder is fixed to the ground, and the top can move horizontally along the traverse mechanism. This model simply mimics an airplane wing under aerodynamic loading. In Fig. 7, both of the control points are marked, and the speckle coat is sprayed so that a simultaneous comparison is made under the same situation. A reference image is shown in Fig. 7a, and an image with a horizontal movement of 2.5 mm (about eight pixels) at the top of the cylinder is shown in Fig. 7b. The displacement vector field is shown in Fig. 8, where the corresponding movement is displayed. The interrogation window of recursive multigrid processing was 16×16 pixels.

Table 1 Quantitative analysis of interpolation methods

Interpolation	Kernel size	MRE, %	Error ratio[a]	Run-time ratio[b]
Nearest neighbor	1×1	3.397	1.712	1.00
Linear	2×2	2.280	1.149	2.81
B-spline	4×4	2.637	1.330	10.58
Cubic	4×4	2.005	1.011	10.24
Cubic	6×6	2.010	1.013	20.03
Truncated sinc	6×6	12.063	6.080	20.08
Windowed sinc	6×6	1.984	1.000	20.19

[a]Error ratio represents the error normalized by the windowed-sinc interpolation error.
[b]Run-time ratio is normalized by the nearest-neighbor interpolation time.

The relative-error distributions are shown in Fig. 9 for the case of linear interpolation. No image registration was made in Fig. 9a, yielding an MRE of 49.80%, whereas a second-order polynomial transform function with 36 control points gives an MRE of 4.31% in Fig. 9b. The conventional method with control points shows a relatively small error except in the boundary region and in the vicinity of the control points, where steep intensity changes occur. The present CBIR method yields an MRE of 2.28% in Fig. 9c. The relative errors inside the model are almost negligible, and those in the boundary region are smaller than those of the conventional method. These results demonstrate that CBIR describes a nonlinear deformation accurately without requiring the use of control points.

C. Interpolation Performance Test

The efficiency and accuracy of several interpolation techniques were evaluated by analyzing their interpolation errors and computing time. Figure 10 shows the relative errors of the interpolation results. The model was the same as that in Fig. 7, and the transform was determined by CBIR. The pixels for which $\varepsilon > 0.1$ are displayed in black. Here, the relative error comprises both the interpolation and transformation errors. In Fig. 10, cubic interpolation and windowed-sinc interpolation show few error pixels, whereas a severely spoiled image was obtained from truncated-sinc interpolation. The nearest-neighbor and B-spline interpolation methods exhibited insufficient accuracy.

For a quantitative comparison, the MREs and the error ratios normalized by the windowed-sinc interpolation error are listed in Table 1. Windowed-sinc interpolation was the most accurate method, yielding an MRE of 1.98%, and cubic interpolations showed comparable accuracy. Although the kernel size is increased, the accuracy is not improved. Linear interpolation exhibited moderate accuracy, yielding an error ratio of 1.15%, whereas B-spline interpolation gave worse results because of its inherent blurring property. Truncated-sinc interpolation gave the poorest result.

The computing time of the interpolation schemes was measured on a Pentium 4-1.7GHz PC. The source programs have been coded using LabVIEW, and the processing time was normalized by that for nearest-neighbor interpolation. The run time required for transformation was three times longer than that for nearest-neighbor interpolation. Basically, the interpolation run time was determined by

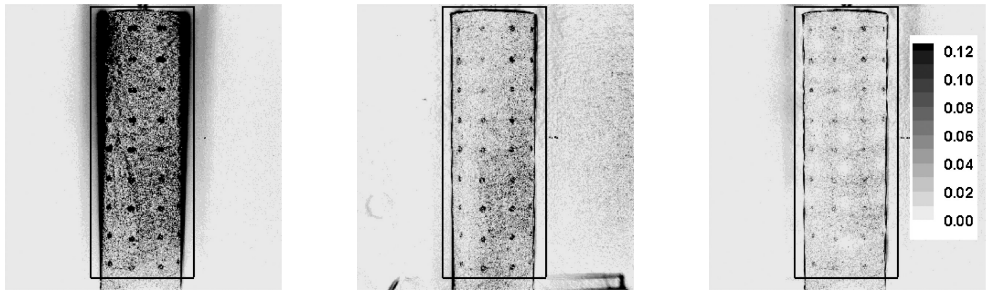

Fig. 9 Relative-error distributions: a) no image registration, b) conventional method, and c) CBIR.

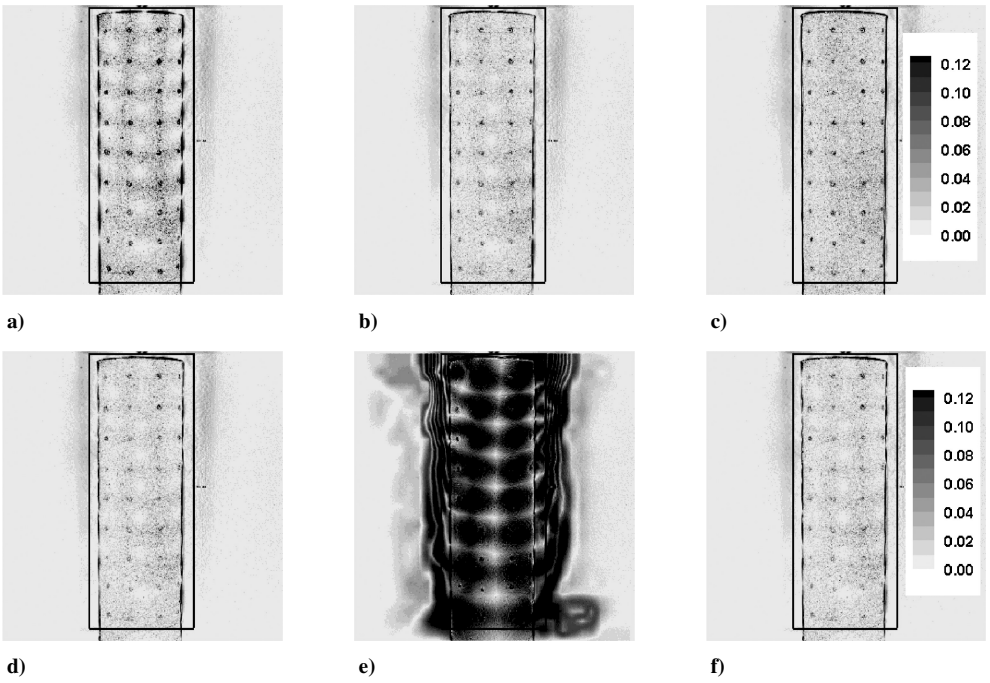

Fig. 10 Relative errors of the interpolation results: a) nearest neighbor, b) linear, c) B-spline, d) cubic (4 × 4), e) truncated sinc, and f) windowed sinc.

the kernel size of the interpolation. Simple methods such as nearest neighbor and linear interpolation were so fast that the interpolation took less time than the transformation itself. The interpolation using a 4×4 kernel size was two times faster than that for a 6×6 kernel. That is, the 4×4 cubic interpolation can save half of the time required by the windowed-sinc interpolation with an additional error of only 1%.

IV. Conclusions

A new algorithm, correlation-based image registration (CBIR), has been developed to improve the resolution of image registration for pressure-sensitive paint. The displacement vectors for the local motion of the model were obtained by calculating the maximum cross correlation between the wind-off and wind-on images. A layer of speckle was sprayed to apply the cross-correlation method in a small interrogation window, without requiring the identification of control points as used in the conventional method. Recursive multigrid processing was employed to increase the nonlinear spatial resolution. It was found that high-resolution images could be obtained by CBIR without requiring control points. The relative-error distributions and the MRE were employed to evaluate the image-registration methods. The conventional method with control points showed a relatively small error, although large errors were produced in the boundary region and in the vicinity of the control points, where steep intensity changes occur. The present CBIR showed relatively small errors and described a nonlinear deformation accurately without control points. Of the interpolation methods evaluated for the image transformation procedure, windowed-sinc interpolation was the most accurate, and 4×4 cubic interpolation was the most efficient. The uncertainty analysis and the spatial noise reduction by filtering process for the present CBIR method will be studied further.

Acknowledgments

This work was partially supported by Hyundai Motor Company and also partially supported by a grant from the National Research Laboratory of the Ministry of Science and Technology, Republic of Korea.

References

[1]Bell, J. H., Schairer, E. T., Hand, L. A., and Mehta, R. D., "Surface Pressure Measurements Using Luminescent Coatings," *Annual Review of Fluid Mechanics*, Vol. 33, 2001, pp. 155–206.

[2]Donovan, J. F., Morris, M. J., Pal, A., Benne, M. E., and Crites, R. C., "Data Analysis Techniques for Pressure and Temperature-Sensitive Paint," AIAA Paper 93-0176, Jan. 1993.

[3]Bell, J. H., and McLachlan, B. G., "Image Registration for Pressure-Sensitive Applications," *Experiments in Fluids*, Vol. 22, No. 1, 1996, pp. 78–86.

[4]McLachlan, B. G., and Bell, J. H., "Pressure-Sensitive Paint in Aerodynamic Testing," *Experimental Thermal and Fluid Science*, Vol. 10, No. 4, 1995, pp. 470–485.

[5]Shanmungasundaram, R., and Samareh-Abolhassani, J., "Modified Scatter Data Interpolation Used to Correct Pressure Sensitive Paint Images," AIAA Paper 95-2041, June 1995.

[6]Le Sant, Y., Deleglise, B., and Mebraki, Y., "An Automatic Image Alignment Method Applied to Pressure Sensitive Paint Measurements," 17th International Congress on Instrumentation in Aerospace Simulation Fascilities, Sept.–Oct. 1997, pp. 57–65.

[7]Weaver, W. L., Jordan, J. D., Dale, G. A., and Navarra, K. R., "Data Analysis for the Development and Deployment of Pressure Sensitive Paints," AIAA Paper 99-0565, Jan. 1999.

[8]Adrian, R. J., "Particle-Imaging Techniques for Experimental Fluid Mechanics," *Annual Review of Fluid Mechanics*, Vol. 23, 1991, pp. 261–304.

[9]Raffel, M., Willert, C. E., and Kompenhans, J., *Particle Image Velocimetry: A Practical Guide*, Springer-Verlag, Berlin, 1998, Chap. 5.

[10]Scarano, F., "Iterative Image Deformation Methods in PIV," *Measurement Science and Technology*, Vol. 13, No. 1, 2002, pp. R1–R19.

[11]Scarano, F., and Riethmuller, M. L., "Iterative Multigrid Approach in PIV Image Processing with Discrete Window Offset," *Experiments in Fluids*, Vol. 26, No. 6, 1999, pp. 513–523.

[12]Jähne, B., *Digital Image Processing*, 5th ed., Springer-Verlag, Berlin, 2002, pp. 269–280.

[13]Lehmann, T. M., Gönner, C., and Spitzer, K., "Survey: Interpolation Methods in Medical Image Processing," *IEEE Transactions on Medical Imaging*, Vol. 18, No. 11, 1999, pp. 1049–1075.

[14]Keane, R. D., and Adrian, R. J., "Theory of Cross-Correlation Analysis of PIV Images," *Applied Science Research*, Vol. 49, No. 3, 1992, pp. 191–215.

K. Fujii
Associate Editor